A Three-Dimensional Finite Element Formulation for the Static Structural Analysis of Bowed Reactor Core of LMFBR

M. Nakagawa

NAIG Nuclear Research Laboratory,
Nippon Atomic Industry Group Co., Ltd., 4-1, Ukishima-cho,
Kawasaki 210, Japan

SUMMARY

A new computational model is presented for the prediction of the displacement profiles in a cluster of subassemblies (core elements) under steady state conditions in LMFBR cores.

This report describes the analytical models and numerical procedures together with some typical results obtained by a prototype code.

In this code, a folded plate structure model is adopted to describe the behavior of reactor hexagonal assemblies more realistically than the beam model which is commonly used in existing codes. The finite element method is employed as the numerical procedure to solve the structural equations. To represent the nonlinear stiffness due to contacts and separations of adjacent ducts, a fictitious finite element (called "joint element") has been newly derived to be placed on contact surfaces with adjacent ducts and with the restraint rings or yokes. The joint element can represent the friction effects, though the present model is as yet preliminary. Furthermore it is able to (adequately) describe the state of partial contact. To construct the mathematical model for the joint element with these functions, a new technique is proposed.

The nonlinearity of the problem due to contact and separation is solved by the step iterative procedure based on the Newton-Raphson method. In each step iterative procedure, the linear equilibrium equations are reconstructed and solved directly. As for the numerical procedure to solve a large set of linear equilibrium equations, the substructure method was adopted to save computer time and memory.

For the qualitative validation of the present formulation, sample calculations were performed on the bundle arrays consisting of two and seven adjacent hexagonal ducts. In these calculations, contact and separation processes under the influences of friction forces, off-center loading, duct torsion, and thermal expansion were analyzed. These results are quite reasonable in the light of the expected behavior.

This work was performed under the sponsorship of Toshiba Corporation.

1. Introduction

In the design and analysis of fast reactor cores, there are a number of problems related to the effects of bowing of reactor assemblies. Structural reactivity effects occur during startup, transients, and long-term usage because the ducts can bow due to temperature, creep, swelling, and elastic pressure deformation effects. Likewise, hexagonally shaped ducts will experience loads due to bowing effects and these loads, stresses, and deformations must be predicted. Effective design requires some analytical methods for the prediction of these effects. At present, such analyses are often performed using computer programs which treat an assembly in a beam model such as NUBOW /1/. However, with this type of codes, it seems difficult to adequately treat the effects of friction forces, off-center loading, duct rotations and torsion, and of the detailed deformation of hexagonally shaped ducts. In the analysis of high-burnup cores, these effects may become important in determining the displacement profiles in a cluster of subassemblies. Hence, the objective of this study is to develop a more detailed analytical code, which allows consideration of the above mentioned effects. As the first step for reaching this aim, we have developed and tested a code ARKAS which simulates the mechanical properties in a cluster of up to seven subassemblies.

In the following chapters, some important features of the program are discussed and then the results of test calculations performed for typical problems are described.

2. Theoretical Formulation

2.1 Analytical Model

2.1.1. Geometrical Model

The geometrical model is illustrated in fig. 1. It is assumed that individual ducts have the folded plate structure consisting of six thin-plates, while individual nozzles are assumed to have the beam structure. Each nodal point has six degrees of displacement freedom : three translational and three rotational.

The joint elements/2/ introduced for representing the nonlinearity due to contact and separation are placed on contact surfaces with adjacent ducts at the user-specified axial locations, and with the restraint rings or yokes which may be included as the outer boundaries of the system.

2.1.2 Physical Model

The continuum is assumed to be a homogeneous, isotropic and elastic material, and adequately described by a small-deformation theory/3/.

The joint element, which is designed with a new technique developed in this study, is expressed under the following assumptions :

(i) There is no resistance against net tension force in the normal direction.
(ii) There is high resistance against compression.
(iii) Shear resistance is proportional to the normal compression.

Although the last assumption is not valid in the light of the actual friction behavior such as stick-slip phenomenon, it is adopted, for the sake of convenience, as the first step of developing the computer code.

2.2 Finite Element Formulation

2.2.1 Derivation of explicit nonlinear equations/4/

Using the virtual work principles, the equilibrium equation, in the presence of contact nonlinearities, initial strains and fluid pressures, is obtained by

$$\int_V \underset{\sim}{B}^T \underset{\sim}{\sigma}\ dV - \int_A \underset{\sim}{N}^T \underset{\sim}{p}\ dA = 0 \tag{1}$$

where the integrals are taken over the whole volume V and over the whole surface area A on which the fluid pressure $\underset{\sim}{p}$ are given. The displacement vector $\underset{\sim}{u}$ and the total strain vector $\underset{\sim}{\varepsilon}$ are expressed in terms of the nodal displacement vector $\underset{\sim}{r}$ as

$$\underset{\sim}{u} = \underset{\sim}{N}\,\underset{\sim}{r} \quad ; \quad \underset{\sim}{\varepsilon} = \underset{\sim}{L}\,\underset{\sim}{u} \equiv \underset{\sim}{B}\,\underset{\sim}{r} \tag{2}$$

where $\underset{\sim}{L}$ is a suitable linear operator, $\underset{\sim}{N}$ is called the displacement shape function, and $\underset{\sim}{B}$ the strain shape function. The stress-strain relation for the continuum element is written as

$$\underset{\sim}{\sigma} = \underset{\sim}{D}_c (\underset{\sim}{\varepsilon} - \underset{\sim}{\varepsilon}_0) \tag{3}$$

where $\underset{\sim}{D}_c$ is an elasticity matrix and $\underset{\sim}{\varepsilon}_0$ is the initial strain vector summing up thermal, swelling, and creep strains. Similar equations for the joint elements are approximated using differential notation as

$$d\underset{\sim}{\sigma} = \underset{\sim}{D}_J\, d\underset{\sim}{\varepsilon} \tag{4}$$

where

$\underset{\sim}{D}_J > 0$ at contact state

$\underset{\sim}{D}_J = 0$ at separated state

Let the following nonlinear equation represent above equations.

$$\underset{\sim}{\sigma} = \underset{\sim}{\tilde{D}}_J\,(\underset{\sim}{r})\,\underset{\sim}{\varepsilon} \tag{5}$$

Substitution of eqs.(2), (3) and (5) into eq.(1) gives explicit nonlinear equations relating total nodal displacement vector $\underset{\sim}{r}$ with total load vector $\underset{\sim}{f}$.

$$(\underset{\sim}{K}_c + \underset{\sim}{\tilde{K}}_J(\underset{\sim}{r}))\,\underset{\sim}{r} = \underset{\sim}{f} \tag{6}$$

where

$$\underset{\sim}{K}_c = \int_{V_c} \underset{\sim}{B}_c^T \underset{\sim}{D}_c \underset{\sim}{B}_c\ dV = \sum_{e=1}^{E_c} \int_{V_c^{(e)}} \underset{\sim}{B}_c^{(e)T} \underset{\sim}{D}_c^{(e)} \underset{\sim}{B}_c^{(e)} dV \tag{7}$$

$$\underset{\sim}{\tilde{K}}_J(\underset{\sim}{r}) = \int_{V_J} \underset{\sim}{B}_J^T \underset{\sim}{\tilde{D}}_J(\underset{\sim}{r})\, \underset{\sim}{B}_J\ dV = \sum_{e=1}^{E_J} \int_{V_J^{(e)}} \underset{\sim}{B}_J^{(e)T} \underset{\sim}{\tilde{D}}_J(\underset{\sim}{r})^{(e)} \underset{\sim}{B}_J^{(e)} dV \tag{8}$$

$$\underset{\sim}{f} = \int_{A_c} \underset{\sim}{N}_c^T \underset{\sim}{p}\ dA + \int_{V_c} \underset{\sim}{B}_c^T \underset{\sim}{D}_c\, \underset{\sim}{\varepsilon}_0\ dV = \sum_{e=1}^{E_c} \left(\int_{A_c^{(e)}} \underset{\sim}{N}_c^{(e)T} \underset{\sim}{p}^{(e)} dA + \int_{V_c^{(e)}} \underset{\sim}{B}_c^{(e)T} \underset{\sim}{D}_c^{(e)} \underset{\sim}{\varepsilon}_0^{(e)} dV \right) \tag{9}$$

The subscript c indicates values corresponding to the contimuum elements, J to the joint elements, and the superscript (e) to the finite element (e).

2.2.2 Linearization of the nonlinear equations/4/

Let us write the nonlinear equation (eq.(6)) as

$$\underset{\sim}{\varphi}(\underset{\sim}{r}) \equiv \underset{\sim}{P}(\underset{\sim}{r}) - \underset{\sim}{f} = 0 \tag{10}$$

Let $\underset{\sim}{r} = \underset{\sim}{r}^n$ be an approximate solution of eq.(6), then we can write an improved solution using a curtailed Taylor expression as

$$\underset{\sim}{\varphi}(\underset{\sim}{r}^{n+1}) \equiv \underset{\sim}{\varphi}(\underset{\sim}{r}^n) + \left(\frac{d\underset{\sim}{\varphi}(\underset{\sim}{r})}{d\underset{\sim}{r}}\right)_n \Delta \underset{\sim}{r}^n = 0 \tag{11}$$

with

$$\underset{\sim}{r}^{n+1} = \underset{\sim}{r}^n + \Delta \underset{\sim}{r}^n \tag{12}$$

In the above

$$\frac{d\,\underset{\sim}{Q}(\underset{\sim}{r})}{d\,\underset{\sim}{r}} \equiv \frac{d\,\underset{\sim}{P}(\underset{\sim}{r})}{d\,\underset{\sim}{r}} \equiv \underset{\sim}{K}_T(\underset{\sim}{r}) \tag{13}$$

represents a tangential matrix. The improved solution can then be obtained by solving the following linear equation for $\Delta \underset{\sim}{r}^n$

$$\underset{\sim}{K}_T(\underset{\sim}{r}^n)\,\Delta \underset{\sim}{r}^n = (\underset{\sim}{f} - \underset{\sim}{P}(\underset{\sim}{r}^n)) \tag{14}$$

The resulting displacement $\underset{\sim}{r}^{n+1}$ leads to a new set of linearized equations, which are solved again for $\Delta \underset{\sim}{r}^{n+1}$. This procedure has to be repeated till the residual force vector reqresented by the right-hand side of eq.(14) becoms nearly equal to zero.

The tangential matrix $\underset{\sim}{K}_T$ is now given by

$$\underset{\sim}{K}_T(\underset{\sim}{r}) \equiv \frac{d\,\underset{\sim}{P}(\underset{\sim}{r})}{d\,\underset{\sim}{r}} = \int_{V_c} \underset{\sim}{B}_c^T \frac{d\,\underset{\sim}{\sigma}}{d\,\underset{\sim}{\varepsilon}} \frac{d\,\underset{\sim}{\varepsilon}}{d\,\underset{\sim}{r}}\, dV + \int_{V_J} \underset{\sim}{B}_J^T \frac{d\,\underset{\sim}{\sigma}}{d\,\underset{\sim}{\varepsilon}} \frac{d\,\underset{\sim}{\varepsilon}}{d\,\underset{\sim}{r}}\, dV = \underset{\sim}{K}_c + \int_{V_J} \underset{\sim}{B}_J^T \underset{\sim}{D}_J \underset{\sim}{B}_J\, dV \equiv \underset{\sim}{K}_c + \underset{\sim}{K}_J(\underset{\sim}{r}) \tag{15}$$

in which eq.(4) is used to eliminate $d\underset{\sim}{\sigma}/d\underset{\sim}{\varepsilon}$. Thus, in addition to the matrices and vectors in eq.(7) and eq.(9), the following matrix is required to solve the nonlinear equation (6) by means of the Newton-Raphson method.

$$\underset{\sim}{K}_J(\underset{\sim}{r}) = \int_{V_J} \underset{\sim}{B}_J^T \underset{\sim}{D}_J \underset{\sim}{B}_J\, dV = \sum_{e=1}^{E_J} \int_{V_J^{(e)}} \underset{\sim}{B}_J^{(e)T} \underset{\sim}{D}_J^{(e)} \underset{\sim}{B}_J^{(e)}\, dV \tag{16}$$

We note that the following relations are required for the calculation of the stiffness matrix with regard to the joint element by using eq.(16).

$$d\,\underset{\sim}{u}^{(e)} = \underset{\sim}{N}_J^{(e)}\, d\,\underset{\sim}{r}^{(e)};\quad d\underset{\sim}{\sigma}^{(e)} = \underset{\sim}{D}_J^{(e)}\, d\underset{\sim}{\varepsilon}^{(e)};\quad d\underset{\sim}{\varepsilon}^{(e)} = \underset{\sim}{L}_J^{(e)}\, d\,\underset{\sim}{u}^{(e)} \equiv \underset{\sim}{B}_J^{(e)}\, d\,\underset{\sim}{r}^{(e)} \tag{17}$$

2.3 Derivation of Stiffness Matrix

2.3.1 Thin-plate Element

For the thin-plate element, the MCLBB element proposed by A. Ghazaleh/5/ is adopted. Although it is a non-conforming element, its convergence has been found by the "patch test".

2.3.2 Joint Element/2/

This section aimes to derive the stiffness matrix of a joint element shown by the last integral form of eq.(16). For brevity the subscript (e) is omitted in this section.

Figure 2 shows the configuration of a joint element in the state of contact condition. Although this element has a finite thickness h, it is assumed that the thickness is small enough to be ignored in solving the equilibrium equations of the system. Both the upper surface ijkl and the lower surface i'j'k'l' correspond to the thin-plate element. For the purpose of considering the partial contact conditions without increasing the number of finite elements, these two surfaces are subdivided into some areas, each of which is called "subdivided zone" in this paper. The local co-ordinates are indicated by x y z.

In addition to the previously mentioned assumptions in Section 2.1.2., the following approximations are adopted.

(i) The integral value for each joint element in eq.(16) is obtained by summing up the integral values with regard to the subdivided zones. And the $\underset{\sim}{D}_J$ takes a constant value in each subdivided zone.

(ii) The infinitesimal displacement at any point within the joint element is obtained by a linear combination of the displacements of the two points on the surfaces just below and above the point.

(iii) The diagonal element k_{zz} in the elasticity matrix $\underset{\sim}{D}_J$, which represents the relation between normal stress and normal strain, is set to a suitable value kn for solving the equilibrium equations.

Since the displacement at any point on the surface is obtained as the product of the

shape function $\underset{\sim}{N}$ and the nodal displacement $\underset{\sim}{r}$, the average displacements of the subdivided zone m are approximated as :

$$\underset{\sim}{u}_{up}^{(m)} = \frac{\int_{A^{(m)}} \underset{\sim}{N}_{up}\ \underset{\sim}{r}_{up}\ dA}{\int_{A^{(m)}} dA} \quad , \quad \underset{\sim}{u}_{low}^{(m)} = \frac{\int_{A^{(m)}} \underset{\sim}{N}_{low}\ \underset{\sim}{r}_{low}\ dA}{\int_{A^{(m)}} dA} \tag{18}$$

where subscripts "up" and "low" indicate the values with regard to the upper and lower surfaces, respectively. Let $w_{up}^{(m)}$ ($w_{low}^{(m)}$) be the translational term of vector $\underset{\sim}{u}_{up}^{(m)}$ ($\underset{\sim}{u}_{low}^{(m)}$) along z axis. And if g is the initial gap of the corresponding joint element, the overlap depth $w^{(m)}$ of the subdivided zone m is readily obtained as

$$w^{(m)} = w_{up}^{(m)} - w_{low}^{(m)} + g \tag{19}$$

Thus, the following criterion is adopted to judge the occurrence of contact.

$$\begin{aligned} w^{(m)} &\leqq 0 \qquad \text{contact state} \\ w^{(m)} &> 0 \qquad \text{separated state} \end{aligned} \tag{20}$$

For the subdivided zone m in a separated state, the integral over zone m is zero because the $\underset{\sim}{D}_J^{(m)}$ is zero from eq.(4). For the subdivided zone m in a contact state, the integral over zone m is derived from the following considerations.

(1) The infinitesimal displacement at any point within the joint element is written in terms of the nodal infinitesimal displacement by means of the above mentioned approximation(ii). Thus, the shape function $\underset{\sim}{N}_J$ is obtained.

(2) From the assumptions illustrated in Section 2.1.2, the stress vector consists of τ_{xz} , τ_{yz} and σ_{zz} , and the strain vector has the corresponding terms. Therefore, the matrix $\underset{\sim}{D}_J^{(m)}$ is represented by the 3×3 diagonal matrix, and each diagonal term is obtained by approximation(iii) and the assumption (iii) in Section 2.1.2.

(3) Because the tangential forces are loaded only on the upper and lower surfaces, the partial derivatives $\partial w/\partial x$ and $\partial w/\partial y$ vanish, where w is the translational displacement along the z axis. This fact is used for the derivation of $\underset{\sim}{L}_J$.

(4) Utilizing the matrix $\underset{\sim}{N}_J$ and $\underset{\sim}{L}_J$, the strain shape function $\underset{\sim}{B}_J$ is readily obtained.

Employing approximation(i) and substituting these matrices into the last integral equation of eq.(16), the element stiffness matrix $\underset{\sim}{K}_J$ is approximated as

$$\underset{\sim}{K}_J = \sum_{m=1}^{M} \int_{A^{(m)}} (\underset{\sim}{N}_{up}, -\underset{\sim}{N}_{low})^T \underset{\sim}{K}^{(m)} (\underset{\sim}{N}_{up}, -\underset{\sim}{N}_{low})\ dA \tag{21}$$

where

$$\underset{\sim}{K}^{(m)} = \begin{bmatrix} k_{xz}^{(m)} & 0 & 0 \\ 0 & k_{yz}^{(m)} & 0 \\ 0 & 0 & k_{zz}^{(m)} \end{bmatrix}$$

$$\begin{aligned} k_{xz}^{(m)} &= k_{yz}^{(m)} = C \cdot \sigma_{zz}^{(m)} \\ k_{zz}^{(m)} &= 0 \qquad \text{when} \quad w^{(m)} > 0 \\ k_{zz}^{(m)} &= k_n \qquad \text{when} \quad w^{(m)} \leqq 0 \end{aligned}$$

In the above, C is the input constant characterzing the shear resistance and $\sigma_{zz}^{(m)}$ is the normal stress.

2.4 Substructure Method

To solve a set of nonlinear equations(6), a new set of linearized equations (14) has to be solved repeatedly till the residual force vector becoms nearly equal to zero. However, eq.(14) involves so many unknowns that it is very difficult to get solution within reasonable computer time and memory. Therefore, the substructure method /4/ /6/ is applied to solve eq.(14)

For brevity let us call the nodes that are common with joint elements the "joint nodes", the Y- and Z- components of freedoms of the joint nodes the "kept freedoms", and the other freedoms the "reduced freedoms". The nodal displacements of nodes except joint nodes are not necessary in reforming eq.(14) at each nonlinear iteration step, because the nonlinear terms in eq.(14) such as $\underset{\sim}{K}_J(\underset{\sim}{r})$ can be obtained only with the displacements of the joint

nodes. Furthermore, because the main terms in the interaction forces between adjacent ducts are the Y-and Z-components for our problem, the freedoms other than the Y- and Z-components of the joint nodes may be eliminated. For that reason, instead of directly solving eq.(14), the following contracted equations consisting of the kept freedoms are solved.

$$\hat{\underset{\sim}{K}}_T(\underset{\sim}{r}_j^n)\,\Delta\underset{\sim}{r}_j^n = (\hat{\underset{\sim}{f}} - \hat{\underset{\sim}{P}}(\underset{\sim}{r}_j^n)) \tag{22}$$

where

$$\hat{\underset{\sim}{K}}_T(\underset{\sim}{r}_j^n) = \sum_{g=1}^{G_B} \hat{\underset{\sim}{K}}_B^{(g)} + \sum_{e=1}^{E_J} \hat{\underset{\sim}{K}}_J^{(e)}(\underset{\sim}{r}_j^{n(e)}) = \sum_{g=1}^{G_B} (\underset{\sim}{K}_{B_{jj}}^{(g)} - \underset{\sim}{K}_{B_{jr}}^{(g)}(\underset{\sim}{K}_{B_{rr}}^{(g)})^{-1}\underset{\sim}{K}_{B_{rj}}^{(g)}) + \sum_{e=1}^{E_J} \underset{\sim}{K}_J^{(e)}(\underset{\sim}{r}_j^{n(e)}) \tag{23}$$

$$\hat{\underset{\sim}{f}} - \hat{\underset{\sim}{P}}(\underset{\sim}{r}_j^n) = \sum_{g=1}^{G_B} (\underset{\sim}{f}_j^{(g)} - \underset{\sim}{K}_{B_{jr}}^{(g)}(\underset{\sim}{K}_{B_{rr}}^{(g)})^{-1}\underset{\sim}{f}_r^{(g)}) - (\sum_{g=1}^{G_B} \hat{\underset{\sim}{K}}_B^{(g)}\,\underset{\sim}{r}_j^{n(g)} + \sum_{e=1}^{E_J} \underset{\sim}{h}^{(e)}(\underset{\sim}{r}_j^{n(e)})) \tag{24}$$

Here subscript j means values with regard to the kept freedoms and r to the reduced freedoms. The superscript(g) indicates values corresponding to the duct (g). The matrix $\hat{\underset{\sim}{K}}_J^{(e)}$ is obtained by eliminating the matrix coefficients corresponding to the reduced freedoms from the matrix $\underset{\sim}{K}_J^{(e)}$. The vector $\underset{\sim}{h}^{(e)}(\underset{\sim}{r}_j^{n(e)})$ is the required force to deform the joint element(e) from the initial state to displacement $\underset{\sim}{r}_j^{n(e)}$. The matrices $\underset{\sim}{K}_{B_{jj}}^{(e)}$, $\underset{\sim}{K}_{B_{jr}}^{(e)}$, $\underset{\sim}{K}_{B_{rr}}^{(e)}$ and $\underset{\sim}{K}_{B_{rj}}^{(e)}$ are the submatrices obtained by means of subdividing the stiffness matrix $\underset{\sim}{K}_B^{(g)}$ for the duct (g) into parts according to the "kept" and "reduced" freedoms.

After the nonlinear solution $\underset{\sim}{r}_j$ is obtained, the reduced freedoms can be calculated as

$$\underset{\sim}{r}_r = \sum_{g=1}^{G_B} \underset{\sim}{r}_r^{(g)} = \sum_{g=1}^{G_B} (\underset{\sim}{K}_{B_{rr}}^{(g)})^{-1}\,(\underset{\sim}{f}_r^{(g)} - \underset{\sim}{K}_{B_{rj}}^{(g)}\,\underset{\sim}{r}_j^{(g)}) \tag{25}$$

3. The Program ARKAS

The program ARKAS was developed to calculate the equilibrium forces and displacements of a series of hexagonal ducts with joint elements/2/ at contact surfaces, when subjected to an imposed set of temperature distributions. For this purpose, a step iterative procedure/4/based on the Newton-Raphson method is applied in which a set of setting and solving of the linear equation is repeated untill the force equilibrium is achieved. To save computer running time and memory requirement, the substructure method/4//6/ is adopted to form the linear equation.

In the present version of ARKAS, the treatment of the entrance nozzle and the effects of burnup are not included. Thus the next steps of development will include :

- — modeling of the entrance nozzle.
- — modifying the friction model to treat the shear failure along the surface of the joint elements.
- — swelling and creep due to neutron fluence.
- — extention to the whole-core code.

4. Sample Calculations

In sample calculations, two-dimensional (y-z) joint elements were adopted because contacts with adjacent ducts generally occur at the load pads whose axial (x-direction) length is short. And their mathematical model can be drived by an analogus method explained in Section 2.3.2.

a) Calculation of two adjacent hexagonal ducts

A sample calculation was performed to analyze the contact and separation processes of two adjacent hexagonal ducts. As indicated in fig.3, a horizontal external force was exerted obliquely (45° from the normal to the surface) on the uppermost part of a surface of the right-hand duct. The force was exerted in five steps with the magnitude being increased by 28.3kg, totalling to 141.5 kg at the final step. Then, another negative force was further exerted

perpendicularly to the same surface in five steps with the magnitude being increased by 20kg. The net final effect is that the Y-component of the combined force is 100 kg and Z-component is zero. The solid lines in fig.4 conceptually shows the expected movement of the top edges of both ducts, while broken lines show fixed bottom ends of the ducts.

The calculated results are shown in fig.5 where solid lines indicate the trajectories corresponding to the additional exertion of the second force. The difference in the Y-values of the two points a and b is caused by the difference due to the initial gap between the two ducts and by the sliding friction after the contact of the two surfaces.

These results are quite reasonable in the light of the expected movement shown in fig.4. Especially, the fact that the point o finally returned to the initial position indicates that the present model adequately simulates the contact and separation processes of hexagonal ducts.

To see the effects of the input constant C characterizing the shear resistance, an additional calculation was performed changing the value of C to 1/10 of the value used in the above mentioned calculation. Results are shown in fig.6 where thick lines indicate the trajectories corresponding to the additional calculation. The effects of the difference in the value of C is clearly seen.

These results indicate that the friction model proposed in this paper can, at least, roughly describe the sliding effect at the contact surface.

b) Calculation of seven adjacent hexagonal ducts

A sample calculation was performed to analyze the displacement profile of seven adjacent hexagonal ducts under following conditions : (1) the position of the bottom edges are fixed, (2) duct No.1 through No.5 are subject to an axially distributed external load due to a common 3-dimensional temperature distribution, causing thermal load in the negative Y-direction, (3) ducts No.6 and No.7 are free from external load, (4) the cluster consisting of these seven ducts is surrounded by a fixed wall with a finite clearance as shown in fig.7.

The calculated results are shown in fig.8 to fig.10. Figure 8 indicates the average duct displacement in the Y-Z plane where solid lines show the movement of the upper and lower load plane, while broken lines show the initial state of the ducts. The distribution of the interaction forces due to the contacts between neighboring ducts and/or fixed boundaries is shown in fig.9 where the areas marked with oblique lines indicate contact zones, and the numerals written in these areas represent the normal forces acting on the contact surfaces in kg per a contact surface. The tangential forces acting on the contact surfaces and their directions are explained by the numerals and arrows on the sides of the above mentioned areas. The deflection shape of the No.1 duct is drawn in fig.10 to show that the eliminated freedoms(marked by o)at the stage of the iterative calculations can be obtained using the results (marked by ■) of the iterative calculations. Although fig.10 shows only the translational displacements to the Y-direction, the other freedoms including the rotational freedoms at all nodal points are also obtained. All of the freedoms are used to obtain the stress distribution required in the creep calculations.

In the above figures, the magnitude and direction of displacements and loading forces are symmetrical with respect to the Y axis, and the deflection shapes of duct No.1 through No.5 are 'S' curve along the X axis. All these results appear to be quite reasonable.

5. Conclusion

A new model has been presented for the analysis of displacement profiles in a cluster of subassemblies under steady state conditions in LMFBR cores.

To test the algorithm of the new model, a prototype program, ARKAS, has been developed and tested, which can simulate the mechanical properties in a cluster of up to seven subassemblies, taking into account the effects of friction forces, partial contact, off-center loading, duct torsion, fluid pressure and of detailed deformation of hexagonally shaped ducts.

From sample claculations, it is confirmed that the model gives quite reasonable results.

6. Aknowledgement

The author is grateful to Mr. A. Yoshii of Japan Business Automation Corporation, and to Mr. T. Takahashi at Toshiba Corporation for their invaluable assistance and considerable skill in coding the computer programs. He would also like to acknowledge Dr. K. Aoki and Mr. I. Komatsu at NAIG Nuclear Research Laboratory, and Mr. Y. Kumaoka and Mr. K. Tarutani at Toshiba Corporation, for their valuable discussions and sustained encouragement.

References

/1/ G.A. Mclennan, "NUBOW: A FORTRAN-IV Program for the Static Elastic Structural Analysis of Bowed Reactor Cores", ANL-8068 (1974).

/2/ R.E. Goodman, R.L. Taylor, and T. Brekke, "A model for the mechanics of jointed rock", Proc. Am. Soc. Civ. Eng., 94, SM3, 637-59, 1968.

/3/ C.L. Dym, and I.H. Shames, "Solid Mechanics: A VARIATIONAL APPROACH", McGraw-Hill, 1973.

/4/ O.C. Zienkiewicz, "The Finite Element Method, 3rd ed.", McGraw-Hill, 1977.

/5/ Abu Ghazaleh, B.N., "Analysis of Plate Type Prismatic Structures." Ph. D. Thesis Presented to the Division of Structural Engineering and Structural Mechanics, University of California, Berkeley in January 1966.

/6/ R.H. Gallagher, "FINITE ELEMENT ANALYSIS: FUNDAMENTALS", Prentice-Hall, INC., 1975.

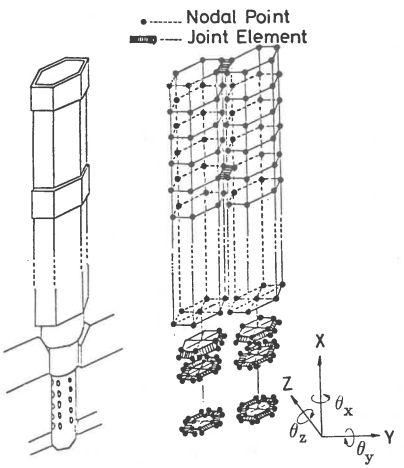

Fig. 1 Schematic Configuration of LMFBR Fuel Assembly and Analysis Model

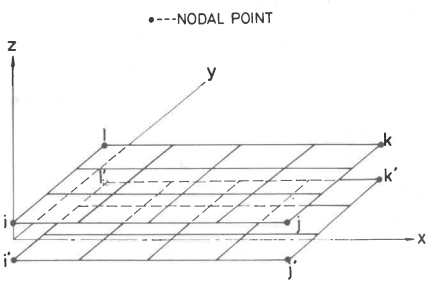

Fig. 2 A Joint Element

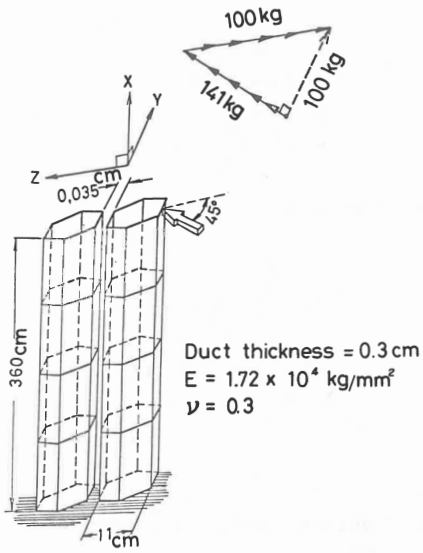

Fig. 3 Geometric Model and Conditions for Sample Calculation (a)

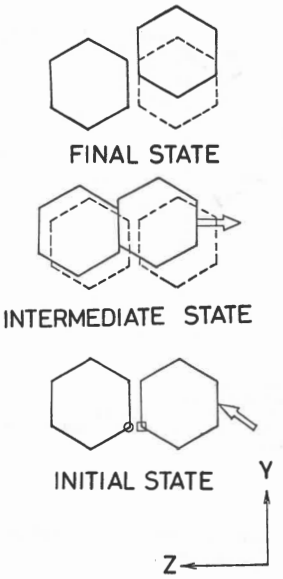

Fig. 4 Expected Movement of the Top Edges of Both Ducts

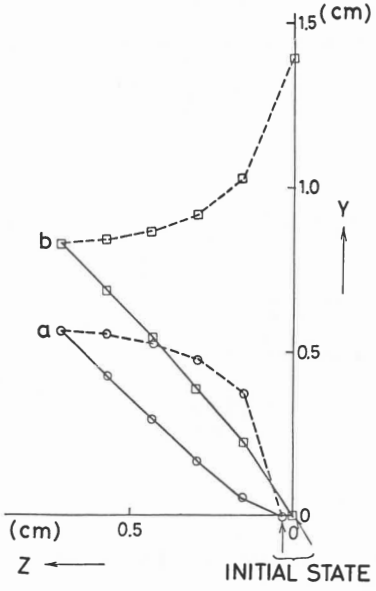

Fig. 5 Calculated Trajectories of the Movement of the Two Points in the Y–Z Plane

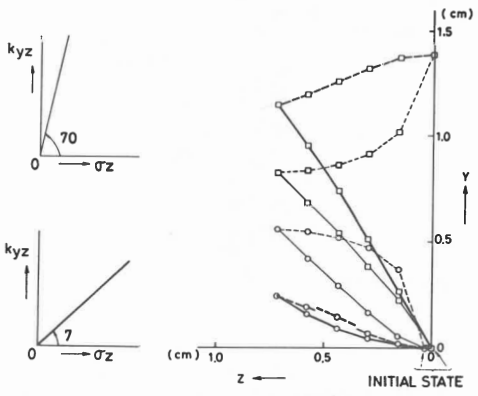

Fig. 6 Effects of the Value of C

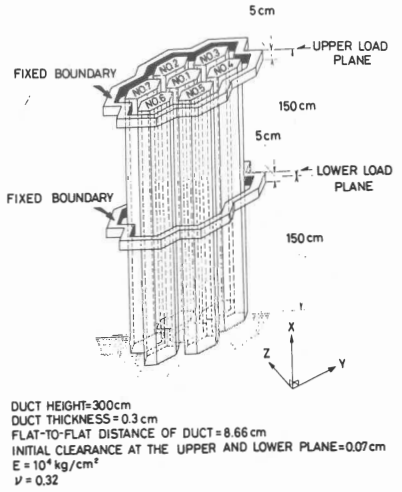

Fig. 7 Geometric Model and Conditions for Sample Calculation (b)

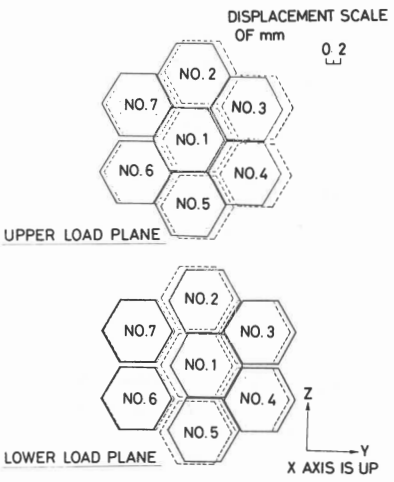

Fig. 8 Deflections at the Upper and Lower Load Planes

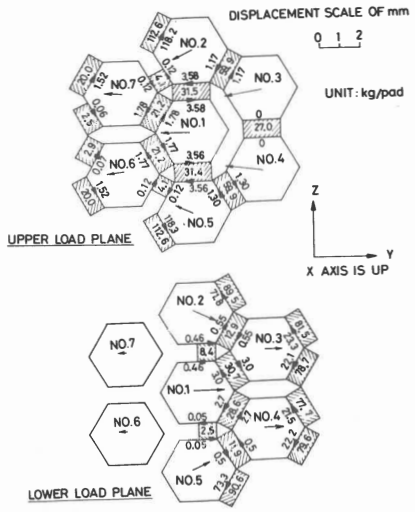

Fig. 9 Distributions of Interaction Forces at the Upper and Lower Load Planes

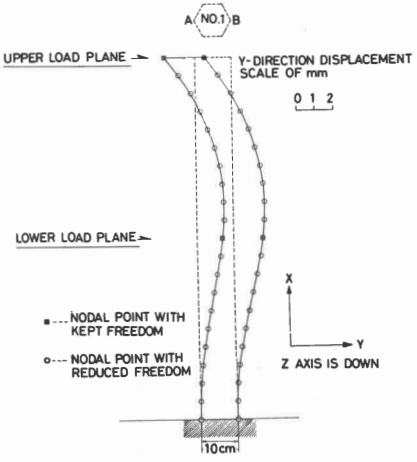

Fig. 10 Deflection of Duct No.1 (with recovered reduced freedoms)